Electronic Supporting Information

Bioinspired Metal-Organic approach to cross-linked functional 3D nanofibrous Hydro and Aero-gels with Effective Mixtures Separation of Nucleobases by Molecular Recognition.

V. G. Vegas,[a] G. Beobide,[b,c] O. Castillo,[b,c] E. Reyes,[d] C. J. Gómez-García,[e] F. Zamora[a,f] and P. Amo-Ochoa*[a,f]

Contact: pilar.amo@uam.es

[a]Department of Inorganic Chemistry, Autonomous University of Madrid, E-28049 Madrid, Spain.

[b]Department of Inorganic Chemistry, University of the Basque Country (UPV/EHU), P.O. Box 644, E-48080, Bilbao, Spain.

[c]BC Materials, UPV/EHU Science Park, Barrio Sarriena s/n, E-48940 Leioa, Spain.

[d]Department of Organic Chemistry II, University of the Basque Country (UPV/EHU), P.O. Box 644, E-48080, Bilbao, Spain.

[e]Instituto de Ciencia Molecular (ICMol), Parque Científico, Universidad de Valencia, Catedrático José Beltrán, 2, 46980 Paterna. Valencia, Spain.

[f]Research in Chemical Sciences at UAM (IADCHEM). Universidad Autónoma de Madrid. 28049 Madrid, Spain.

Experimental procedures

Materials and Methods

4,4´-bipyridyl (4,4-bipy) 98 %, copper acetate monohydrate extra pure; sodium hydroxide and glacial acetic acid were purchased from standard chemical suppliers and were used as received. The ligand uracil-1-acetic acid (UAcOH) was synthesized as described in the literature.[1]

Infrared (IR) spectra were recorded on a PerkinElmer 100 spectrophotometer using a PIKE Technologies MIRacle Single Reflection Horizontal ATR Accessory from 4000–600 cm^{-1}.

Elemental analyses were performed on an elementary microanalyzer LECO CHNS-932, working with controlled doses of O_2 and a combustion temperature of 1000 °C.

Powder X-ray diffraction patterns have been collected using a Bruker D8 Advance X-ray diffractometer (Cu-Kα radiation; $\lambda = 1.5418$ Å) equipped with a Lynxeye detector. Samples were mounted on a flat glass plate and analysed with scanning $\theta/2\theta$. Theoretical X-ray powder diffraction patterns were calculated using Mercury CSD 4.2.0 software from the Crystallographic Cambridge Data Base (CCDC).

The single crystal X-ray diffraction data collection and structure determination for compound **1** was done at 296 K on a Bruker Kappa Apex II diffractometer with graphite-monochromated (Mo-K_α radiation; $\lambda = 0.71073$ Å). The cell parameters were determined and refined by a least-squares fit of all reflections. A semi-empirical absorption correction (SADABS) was applied. The structure was solved by direct methods using the SIR92 program[2] and refined by full-matrix least-squares on F^2 including all reflections (SHELXL).[3,4] Crystal parameters and details of the final refinements of compound **1** are summarized in Table S1. The hydrogen atoms were included in their calculated positions and refined riding on the respective carbon atoms. All calculations were performed using the WINGX crystallographic software package.[5] CCDC deposition number: 1988473.

Thermogravimetric analysis (TGA) was performed on a TGA Q500 Thermobalance equipped with an EGA (Evolved Gas Analysis) furnace and quadrupole mass spectrometer (Thermostat Pfeiffer of Tecnovac) to analyse gases being released from the sample. The powder sample was analysed using a Pt sample holder and O_2 flow as purge gas (90 mL/min) with a heating ramp from room temperature to 1000 °C at 5 °C/min.

Magnetic measurements were done in a Quantum Design MPMS-XL-5 SQUID magnetometer in the 2-300 K temperature range with an applied magnetic field of 0.1 T on a polycrystalline sample of compound **1n** (with a mass of 13.155 mg). Isothermal magnetization measurements were performed on the same sample at 2 K with magnetic fields in the range 0-5 T. The susceptibility data were corrected for the sample holder, previously measured under the same conditions, and for the diamagnetic contributions as deduced by using Pascal´s constant Tables.[6]

Field emission scanning electron microscopy (FESEM) images were recorded on a Philips XL30 S-FEG field emission scanning electron microscope, and on Carl Zeiss SUPRA 55 scanning electron microscope. The surfaces used for FESEM were SiO_2 300 nm thickness (IMS Company). SiO_2 surfaces were sonicated in ultrasound bath at 37 KHz and 380 Watts, for 15 min in acetone, 15 min in 2-propanol and then dried under an argon flow. *FESEM Sample preparation.* Diluted suspension of compound **1n** was prepared by adding 20 µL of the original suspension (10 mM) over 400 µL of Milli-Q water. 10 µL of the diluted suspension were deposited on SiO_2 substrates by drop casting and allowed to adsorb for 15 min at room temperature. The remaining suspension was removed blowing with an argon flow. Small fragments of **1n-Aerogel** and **1n-Xerogel** were deposited directly over carbon tape.

Atomic Force Microscope (AFM) images were acquired in dynamic mode using a Nanotec Electronica system (www.nanotec.es) operating at room temperature in ambient air conditions. For AFM measurements, Olympus cantilevers were used with a nominal force constant of 0.75 N/m and a resonance frequency of about 70 kHz. The images were processed using WSxM. The surfaces used for AFM were SiO_2 300 nm thickness (IMS Company). SiO_2 surfaces were sonicated in ultrasound bath at 37 Khz and 380 Watts, for 15 min in acetone, 15 min in 2-propanol and then dried under an argon flow. *AFM Samples preparation.* Diluted suspension of compound **1n** was prepared by adding 20 µL of the original suspension (10 mM) over 400 µL of Milli-Q water. Suspensions of 9.5 mg of **1n-Aerogel** in 1 mL of Milli-Q water and 6.5 mg of **1n-Xerogel** in 1 mL of Milli-Q water were also prepared. The corresponding mixtures were stirred for 5 seconds. 15 µL of the diluted suspensions were deposited on SiO_2 substrates by drop casting and allowed to adsorb for 15 min at room temperature. The remaining suspension was removed blowing with an argon flow.

Dinitrogen (77 K) physisorption data were measured on outgassed samples with a Quantachrome Autosorb-iQ-MP. True density of outgassed samples was determined by an automatic helium microultrapycnometer of Quantachrome Instruments. In both cases the outgassing of the samples was conducted by subjecting the samples to 333 K under vacuum for 46 h. A INSTRON 5967 testing device with a 20 N load cell was used to record compression-strain curves using cylindrical specimens of an approximated diameter of 20–25 mm and a length of 10 to 13 mm. Test pieces were compressed to a maximum stress of 18 N at a rate of 5 mm min^{-1}.

Synthesis

Synthesis of $[Cu_2(UAcO)_2(4,4'\text{-bipy})_2(CH_3COO)_2]_n\cdot 3H_2O$ (1) and $[Cu_2(UAcO)_4(4,4'\text{-bipy})_2]_n\cdot 3H_2O$

A mixture of UAcOH (140 mg, 0.82 mmol) in 4 mL of water and NaOH (33 mg, 0.82 mmol) in 3 mL of water was added to a water solution (4 mL) of 4,4'-bipy (64 mg, 0.41 mmol) under stirring at room temperature. The resulting clear solution turned onto a purple colloid upon addition of 3 mL of water solution of $Cu(CH_3COO)_2\cdot H_2O$ (82 mg, 0.41 mmol) (pH = 5.8). The purple colloid, which correspond to $[Cu_2(UAcO)_4(4,4'\text{-bipy})_2]_n\cdot 3H_2O$ 1D coordination polymer (manuscript in preparation, 38 % yield), was stirred for 1 hour at 1200 rpm and the mixture filtered off. Dark blue crystals of **1** were isolated, from the mother liquor upon standing 1 week at 20°C. Then, the dark blue crystals were filtered, washed with water, ethanol and diethyl ether and dried in air (0.056 mg, 15 % yield based on Cu). Anal. Calcd. (found) for $C_{18}H_{22}CuN_4O_9$ (**1**): C, 45.52 (44.14); H, 4.00 (4.18); N, 11.80 (11.93) and IR selected data: 3425 (w), 3092 (w), 3058 (w), 1671 (s), 1607 (s), 1460 (m), 1377 (s), 1328 (s), 1250 (m), 1220 (m), 1078 (m), 961 (m), 814 (s), 764 (m), 725 (m), 676 (m), 637 (m).

Synthesis of 1 with nanometric dimensions (1n) and as a Metal Organic Gel (MOG) (1n-Hydrogel)

A mixture of 4,4'-bipy (64 mg, 0.41 mmol) in CH_3COOH (0.07 mL, 1.23 mmol) was added to a solution of UAcOH (70 mg, 0.41 mmol) in 4 mL of water and NaOH (16.4 mg, 0.41 mmol) in 3 mL of water. The resulting solution turned onto a purple colloid upon addition of 3 mL of an aqueous solution of $Cu(CH_3COO)_2\cdot H_2O$ (82 mg, 0.41 mmol) (pH = 4.5). The optimum hydrogel of **1n**, **1n-Hydrogel**, is formed upon stirring the **1n** purple colloid for 20 min in the ultrasound bath (37 KHz, 380 W) and leaving the sample 24h at room temperature. X-ray powder diffraction confirm the phase purity of the sample **1n** (Fig. S1).

Synthesis of Metal Organic Aerogel (MOA) (1n-Aerogel) and Metal Organic Xerogel (MOX) (1n-Xerogel)

Metal Organic Xerogel (**1n-Xerogel**) was prepared drying **1n-Hydrogel** in open-atmosphere. (0.142 mg, 69 % yield based on Cu). IR selected data: 3425 (w), 3092 (w), 3058 (w), 1671 (s), 1607 (s), 1460 (m), 1377 (s), 1328 (s), 1250 (m), 1220 (m), 1078 (m), 961 (m), 814 (s), 764 (m), 725 (m), 676 (m), 637 (m). X-ray powder diffraction confirm the phase purity of the sample (Fig. S2).

To prepare the metal-organic aerogel (**1n-Aerogel**), an E3100 critical point dryer from Quorum Technologies equipped with gas inlet, vent, and purge valves, and with a thermal bath, was employed. First, several solvent exchanges cycles were performed in the **1n-Hydrogel** to replace water solvent by ethanol. Then, the metallogel was immersed in liquid CO_2 at 293 K and 50 bar for 1 hour. Then, the exchanged ethanol was removed through the purge valve. This process was repeated five times. Subsequently, the sample was dried under supercritical conditions, increasing the temperature and pressure to 313 K and 85−95 bar. Finally, under constant temperature (313 K), the chamber was slowly vented up to atmospheric pressure to achieve **1n-Aerogel**. (0.158 mg, 77 % yield based on Cu)**.** IR selected data: 3425 (w), 3092 (w), 3058 (w), 1671 (s), 1607 (s), 1460 (m), 1377 (s), 1328 (s), 1250 (m), 1220 (m), 1078 (m), 961 (m), 814 (s), 764 (m), 725 (m), 676 (m), 637 (m). X-ray powder diffraction confirm the phase purity of the sample (Fig. S2).

Structural characterization of 1, 1n, 1n-Hydrogel, 1n-Aerogel and 1n-Xerogel

Table S1. Single-crystal data and structure refinement details for compound **1**.

	1
Empirical formula	$C_{18}H_{22}CuN_4O_9$
M_r	501.93
Crystal system	Orthorhombic
Space group	*Fdd2*
a/Å	21.561(3)
b/Å	35.637(5)
c/Å	11.1216(17)
V/Å^3	8545(2)
Z	16
D_c/Mg·m^{-3}	1.561
Color	Dark blue
Crystal habit	Platy
Crystal size/mm^3	0.37 x 0.18 x 0.02
μ/mm^{-1}	1.081
$2\theta_{max}$/º	50.69
Reflections collected	21054
Independent reflections	3823
R_{int}	0.1207
Variable parameters	290
$R1[I>2\sigma(I)]/wR2$[all data][a]	0.0570/0.1089
Goodness-of-fit (F^2)	1.034
$\Delta\rho_{max/min}$/e Å^{-3}	0.709, -0.491

[a] $R1 = \Sigma||F_o| - |F_c|| / \Sigma|F_o|$; $wR2 = [\Sigma[w(F_o^2 - F_c^2)^2] / [\Sigma(F_o^2)^2]]^{1/2}$ where $w = 1/[\sigma^2(F_o^2)+(AP)^2+(BP)]$ with A = 0.0645 (**1**), and B = 0.0000 (**1**).

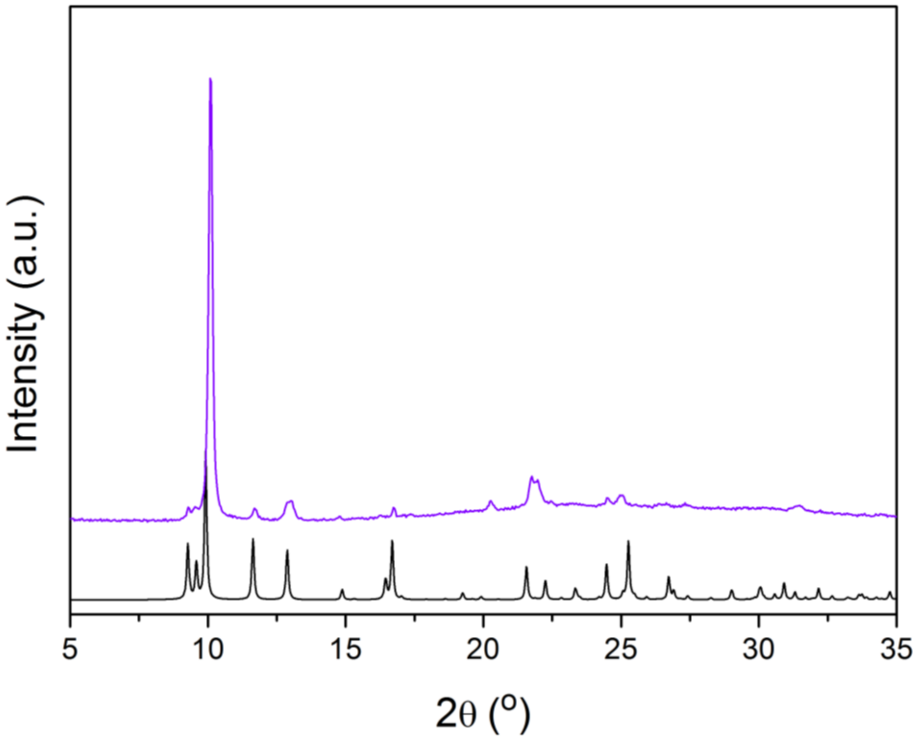

Fig. S1 X-ray powder diffraction patterns of simulated from single crystal structure (black line) and compound **1n** (purple line).

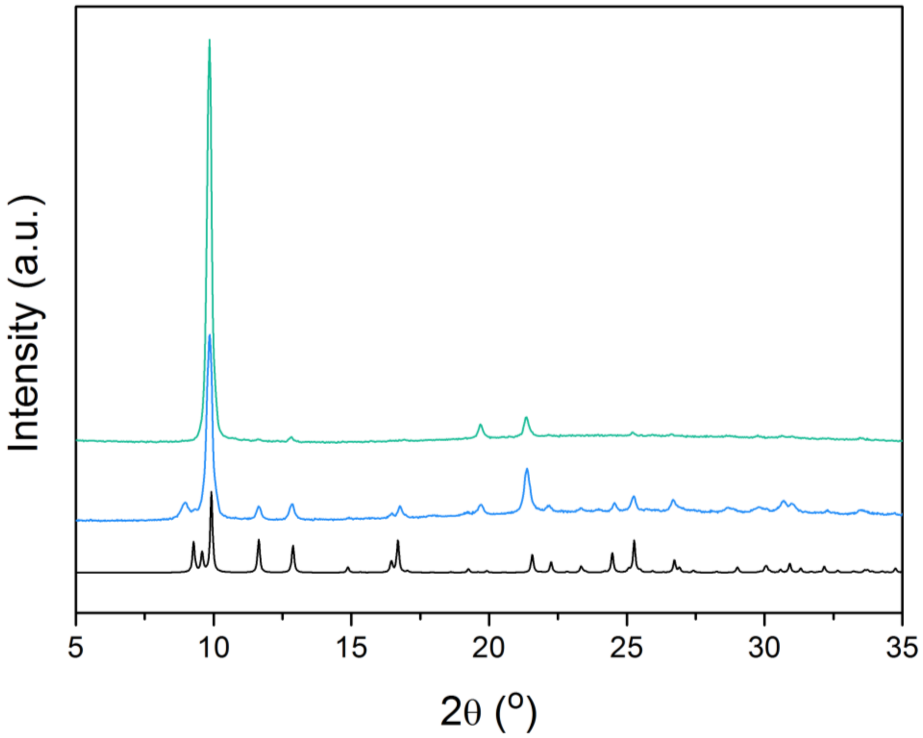

Fig. S2 X-ray powder diffraction patterns of simulated from single crystal structure (black line), **1n-Aerogel** (blue line) and **1n-Xerogel** (green line). As expected, the preferred orientation effect is more pronounced as the sample shrinkages compare the diffractograms of the aerogel (ultralight) and xerogel (highly densified).

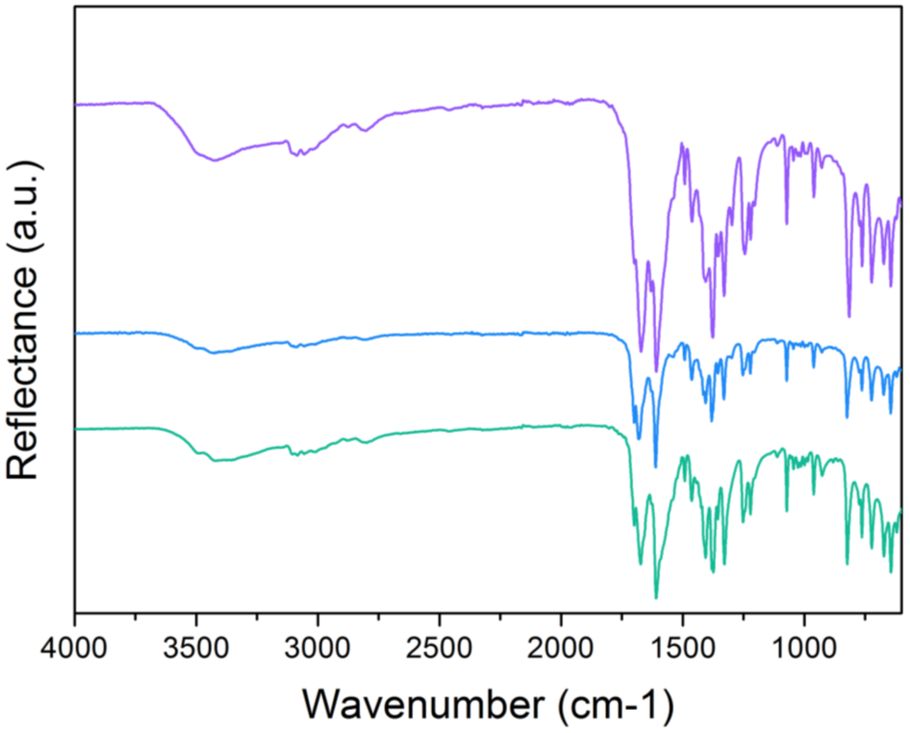

Fig. S3 FTIR spectra of **1n** (purple line), **1n-Aerogel** (blue line) and **1n-Xerogel** (violet line) recorded on ATR mode**.**

Table S2. Hydrogelation studies.

HYDROGEL FORMATION		
STOICHIOMETRY (Cu (II) acetate:Acetic Acid)	**pH**	
1:1	**5.61**	**Unconsolidated Hydrogel**
1:2	**5.51**	**Unconsolidated Hydrogel**
1:3	**5.16**	**Optimum Hydrogel**
1:4	**4.92**	**Unconsolidated Hydrogel**
TEMPERATURE		
15 °C<	**Colloidal Suspension**	
15-30 °C	**Optimum Hydrogel**	
>30 °C	**-**	
TIME		
24h<	**Unconsolidated Hydrogel**	
24h	**Optimum Hydrogel**	

Magnetic Studies

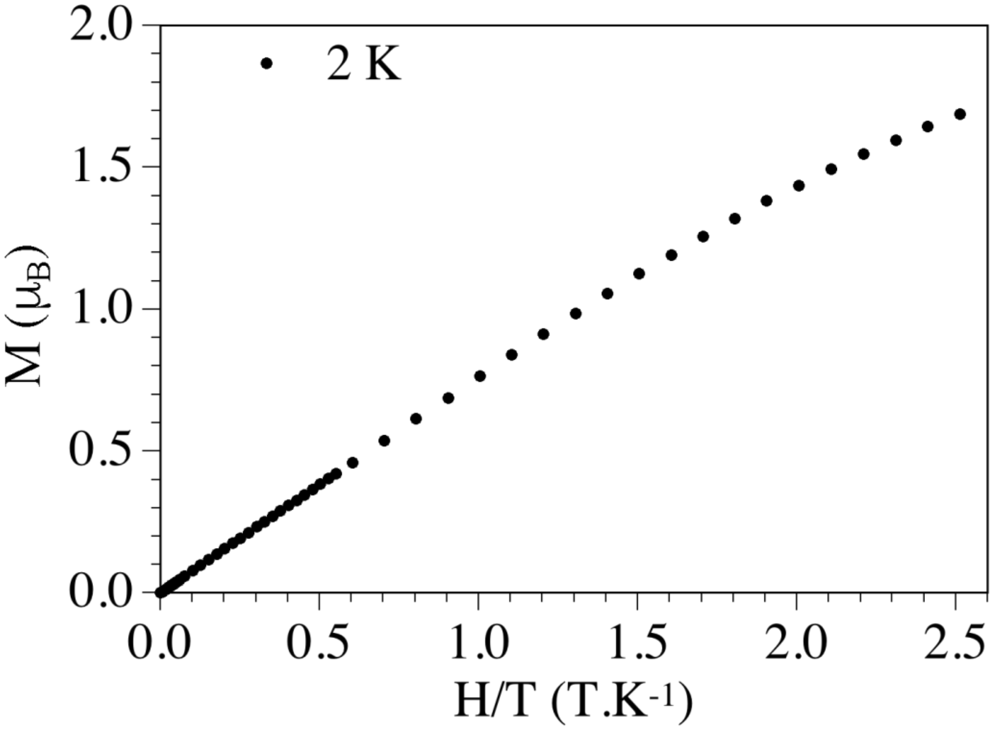

Fig. S4 Isothermal magnetization at 2 K of compound **1n**.

Morphological Study of 1n, 1n-Aerogel and 1n-Xerogel

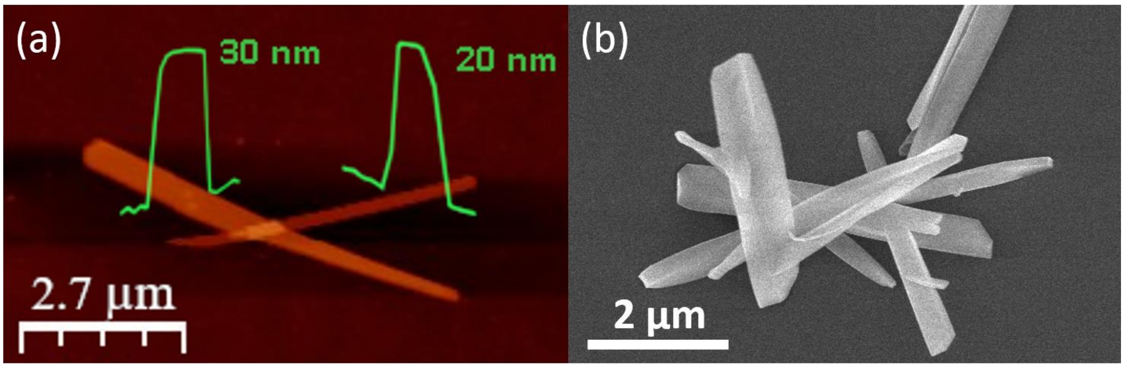

Fig. S5. (a) AFM image of **1n** drop-casted deposited on SiO_2 and the height profiles along the green lines.(b) FESEM image of **1n**.

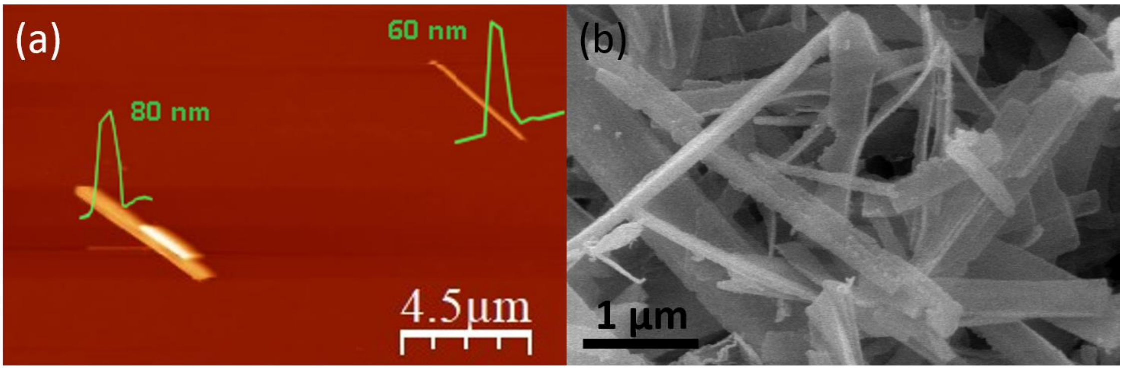

Fig. S6 (a) AFM image of **1n-Aerogel** drop-casted deposited on SiO_2 and the height profiles along the green lines.(b) FESEM image of **1n-Aerogel**.

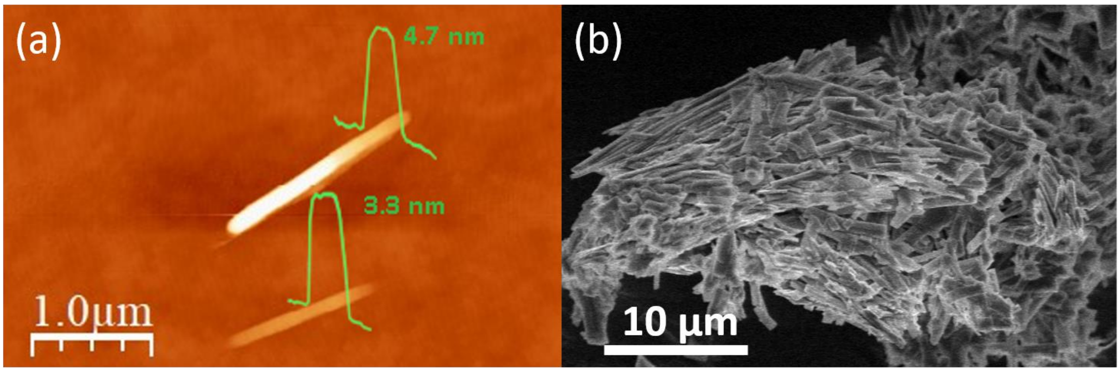

Fig. S7 (a) AFM image of **1n-Xerogel** drop-casted deposited on SiO_2 and the height profiles along the green lines.(b) FESEM image of **1n-Xerogel**.

Chemical Stability Studies of 1n, 1n-Hydrogel, 1n-Aerogel and 1n-Xerogel

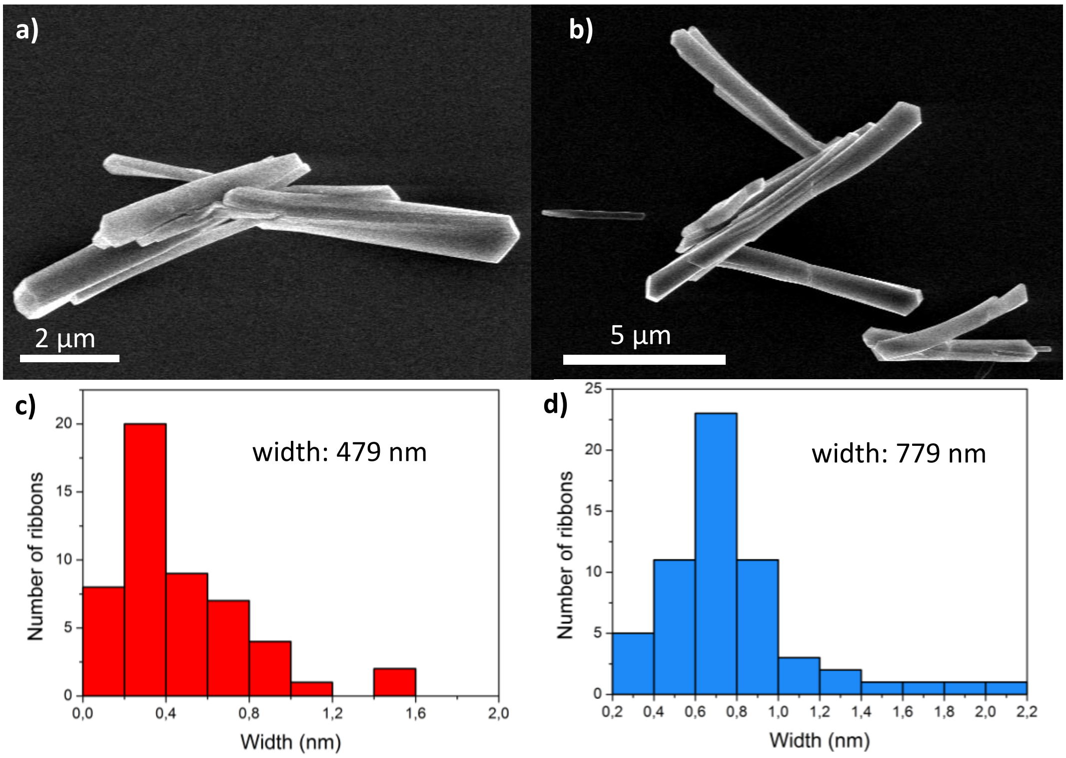

Fig. S8 FESEM images of compound **1n**: a) freshly prepared and b) after one month and the respective histograms of the width below.

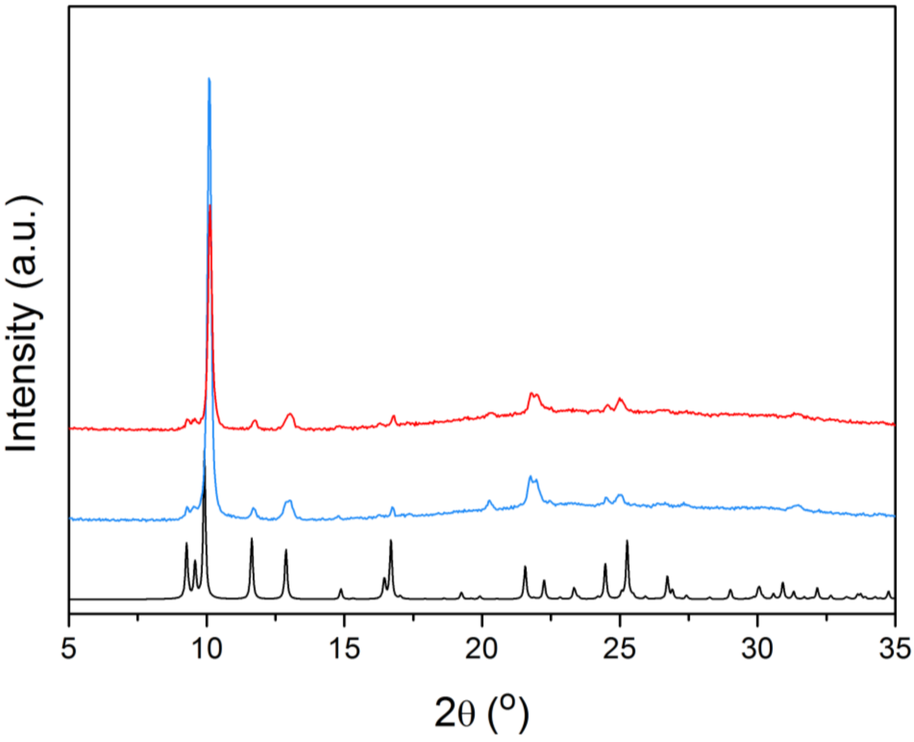

Fig. S9 X-ray powder diffraction patterns of simulated from single crystal structure (black line), **1n** freshly prepared (blue line) and **1n** (red line) after one month.

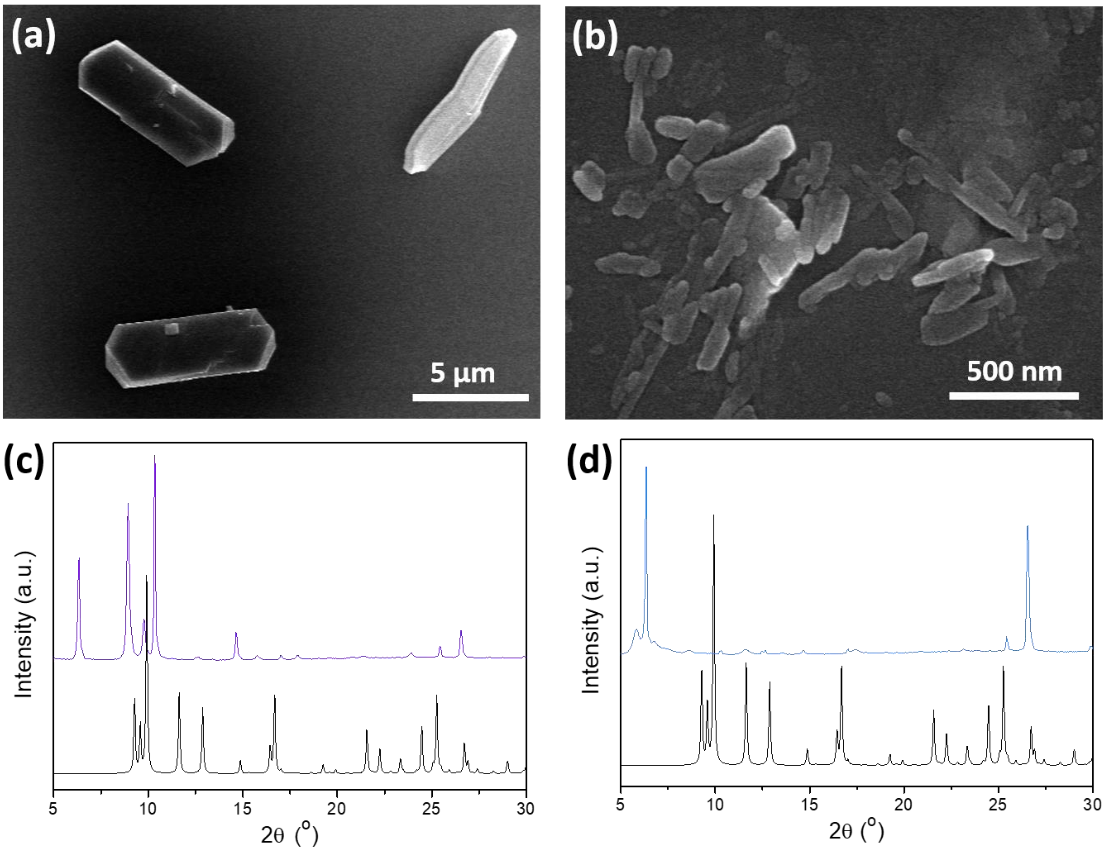

Fig. S10 FESEM images of compound **1n** at: (a) pH = 4.5 and (b) at pH = 6.0. Compound **1n** is transformed after 24 hours at pH 4.5 and 6 (c-d). Compound **1n** was immersed in 3 mL of two buffer solutions at pH 4.5 and pH 6.5 during 24h.

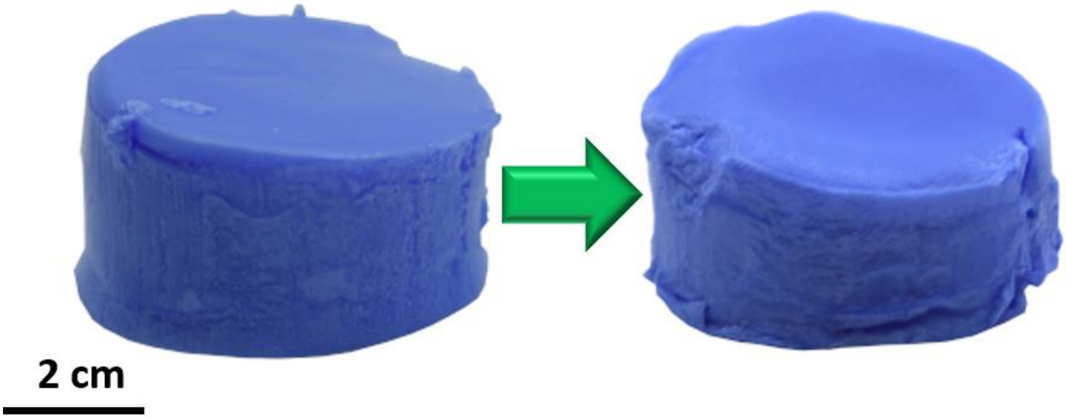

Fig. S11 Monolith **1n-Hydrogel** freshly prepared (left) and one month later (right). The monolith preserves its morphology and its dimensions. **1-Hydrogel** was storage at 25 °C, in EtOH, for one month and compare with the compound freshly obtained.

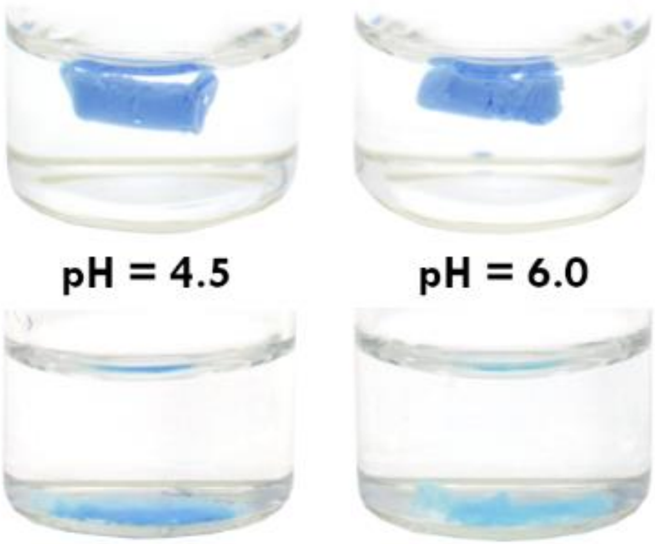

Fig. S12 Fragments of compound **1n-Hydrogel** immersed at pH = 4.5 (left) and pH = 6.0 (right) buffer solutions at 25 °C recently prepared (up) and after 24h (down). **1n-Hydrogel** was immersed in 3 mL of two buffer solutions at pH = 4.5 and pH = 6.5 during 24h.

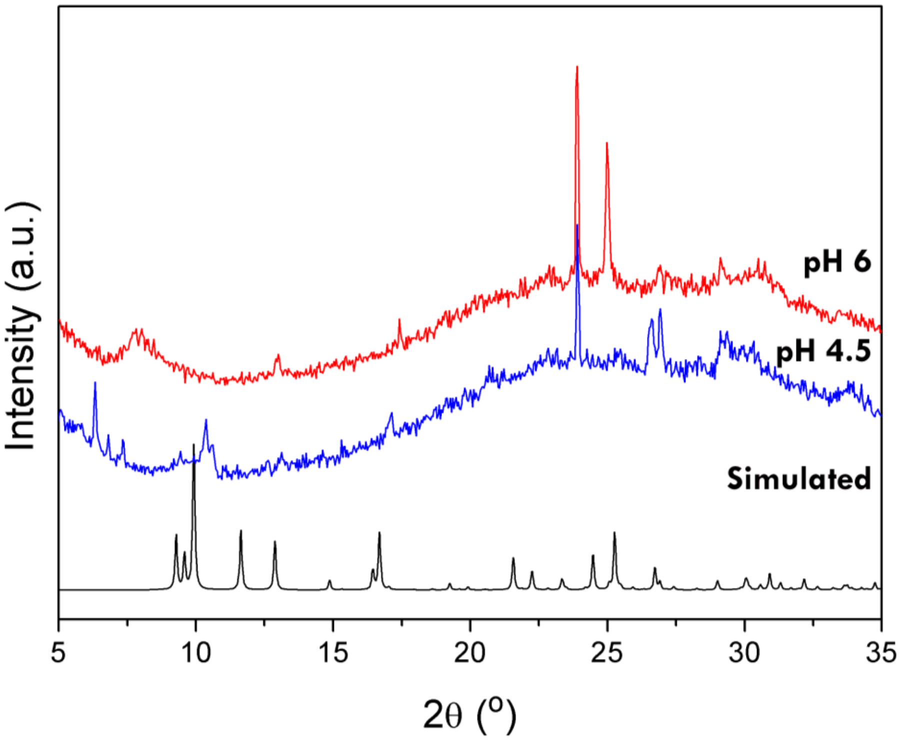

Fig. S13 X-ray powder diffraction patterns of simulated from single crystal structure and **1n-Hydrogel** after 24h immersed at pH 4.5 and pH 6.0 buffer solutions at 25 °C.

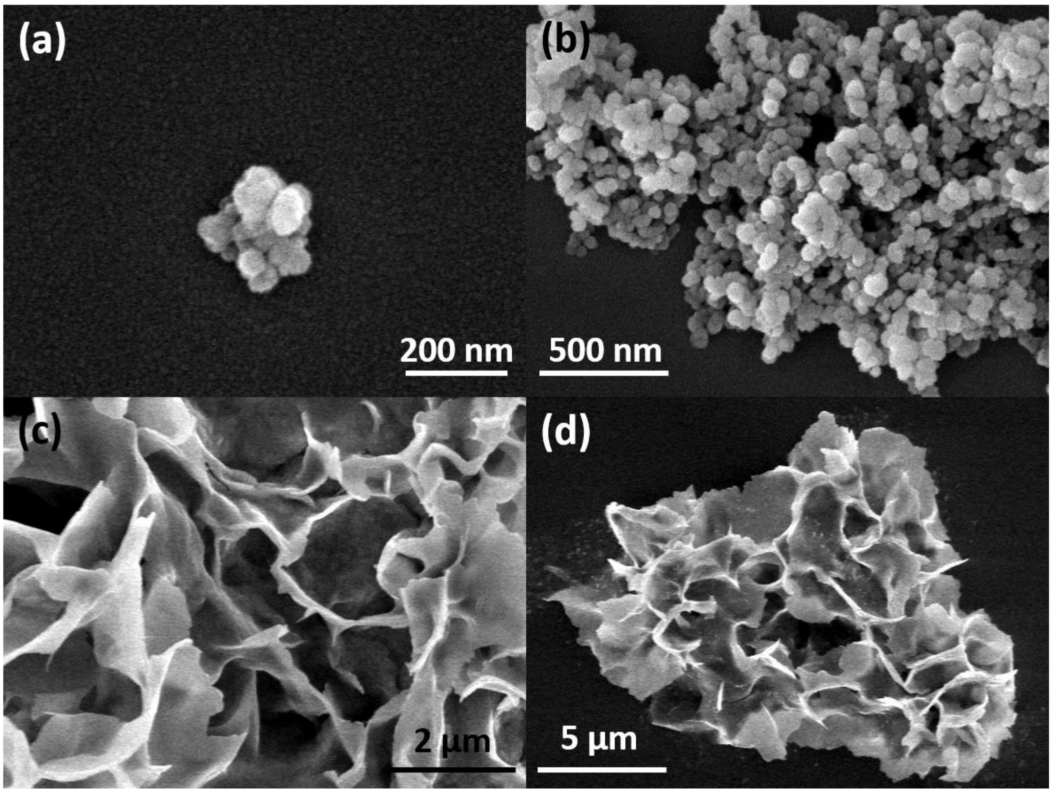

Fig. S14 FSEM images of **1n-Hydrogel** after 24h immersed at pH 4.5 (a,b) and pH 6.0 (c,d) buffer solutions at 25 °C.

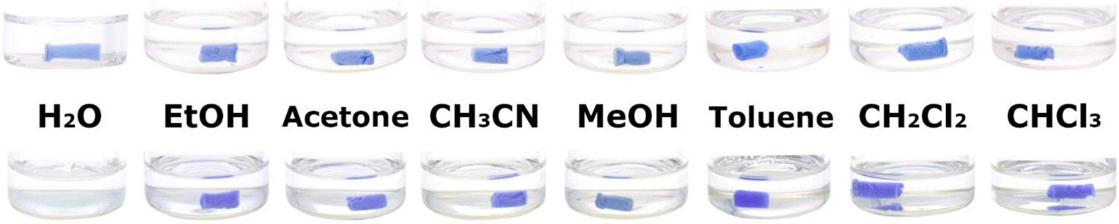

Fig. S15 1n-Hydrogel immersed in different solvents recently prepared (up) and after one week (down).

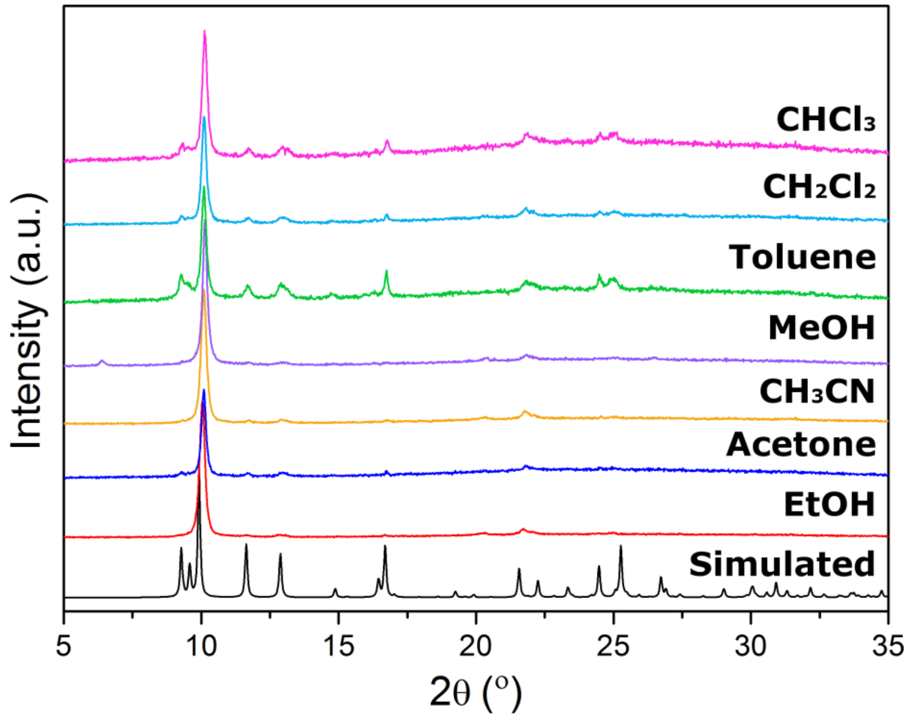

Fig. S16 X-ray powder diffraction patterns of simulated and **1n-Hydrogel** after 1 week immersed in different solvents

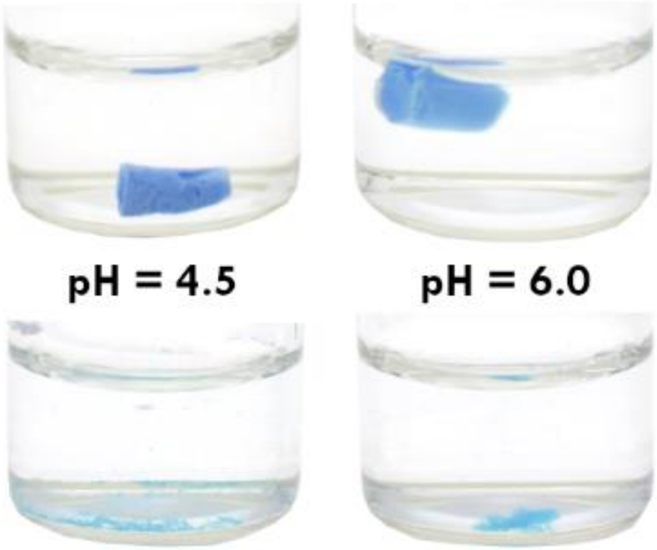

Fig. S17. Fragments of compound **1n-Aerogel** immersed at pH = 4.5 (left) and pH = 6.0 (right) buffer solutions at 25 ºC freshly prepared (up), after 24h (down). **1n-Aerogel** was immersed in 3 mL of two buffer solutions at pH 4.5 and pH 6.5 during 24h.

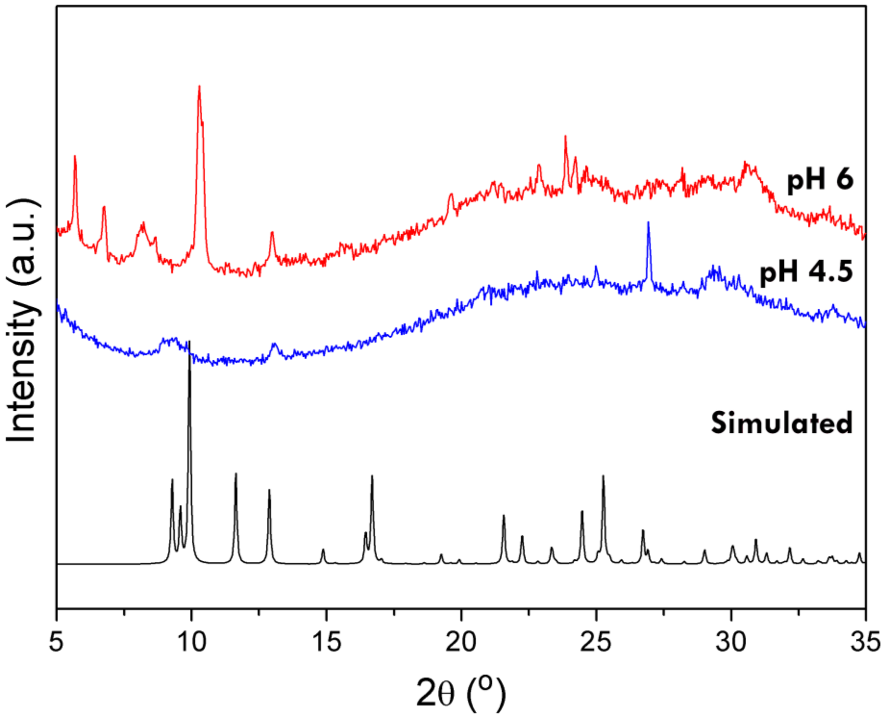

Fig. S18 X-ray powder diffraction patterns of simulated and **1n-Aerogel** after 24h immersed at pH 4.5 and pH 6.0 buffer solutions at 25°C.

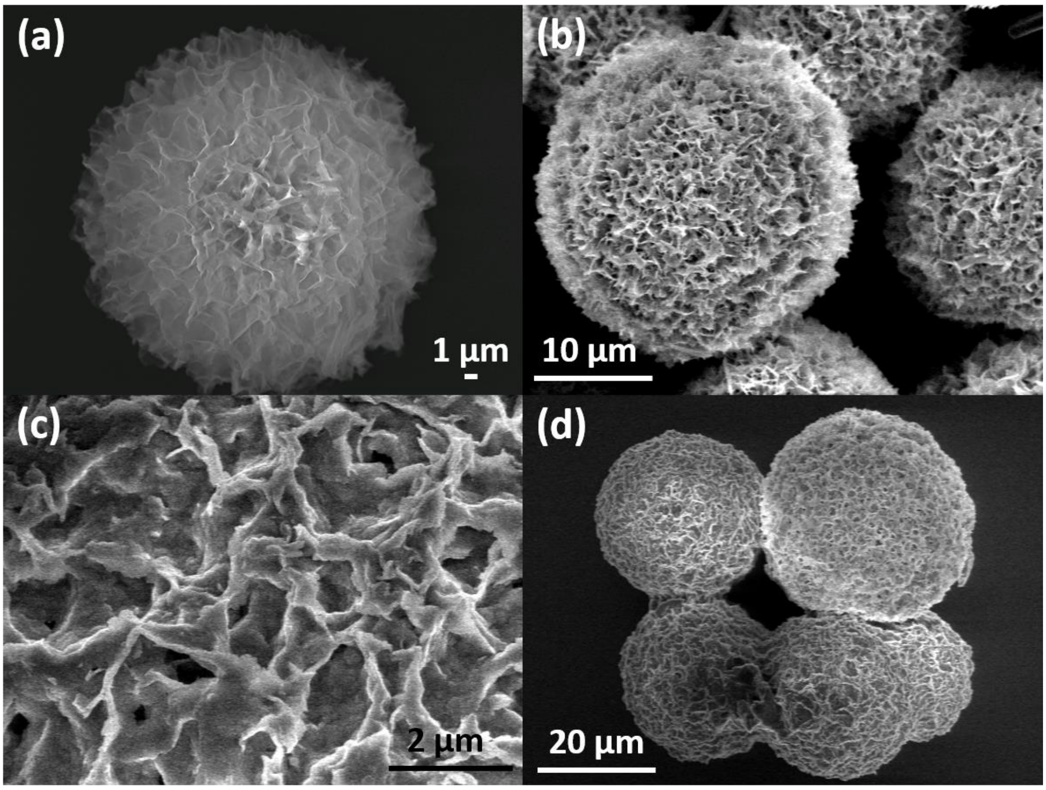

Fig. 19 FSEM images of **1-Aerogel** after 24h immersed at pH 4.5 (a, b) and pH 6.0 (c, d) buffer solutions at 25°C.

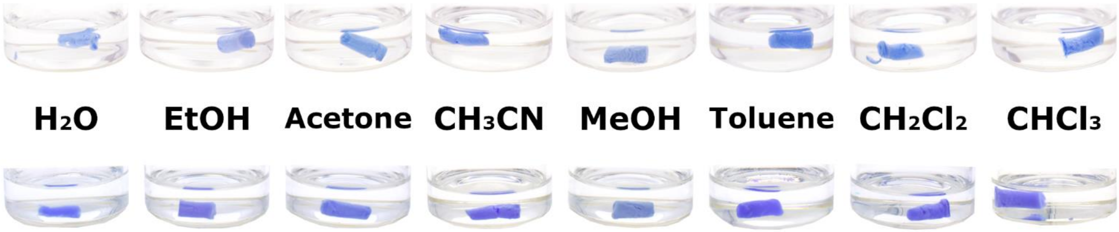

Fig. S20 1n-Aerogel immersed in different solvents recently prepared (up) and after one week (down).

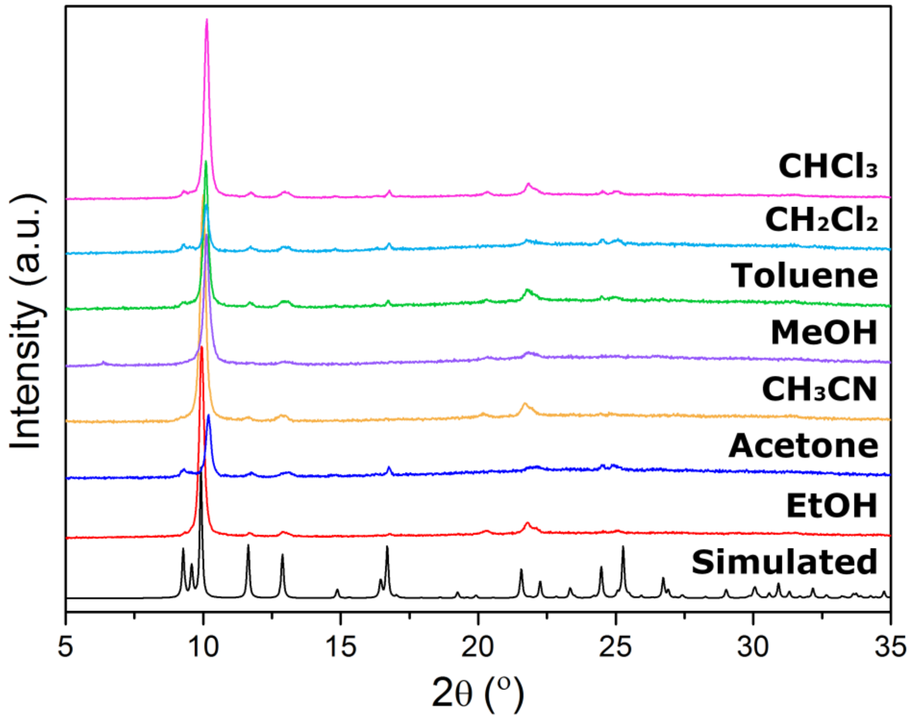

Fig. S21 X-ray powder diffraction patterns of simulated and **1n-Aerogel** after 1 week immersed in different solvents.

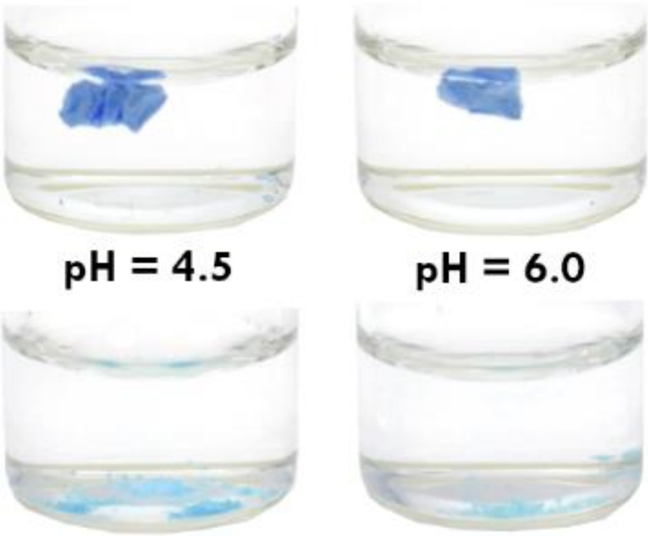

Fig. S22 Fragments of compound **1-Xerogel** immersed at pH = 4.5 (left) and pH = 6.0 (right) buffer solutions at 25 °C freshly prepared (up), after 24h (down). **1n-Xerogel** was immersed in 3 mL of two buffer solutions at pH 4.5 and pH 6.5 during 24h.

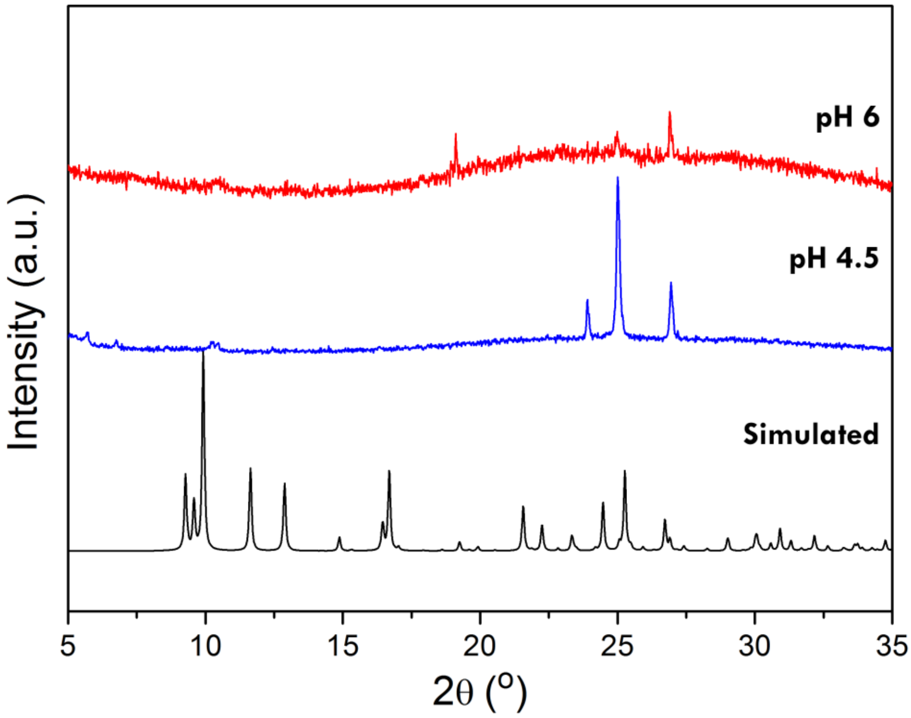

Fig. S23 X-ray powder diffraction patterns of simulated and **1n-Xerogel** after 24h immersed at pH 4.5 and pH 6.0 buffer solutions at 25 °C.

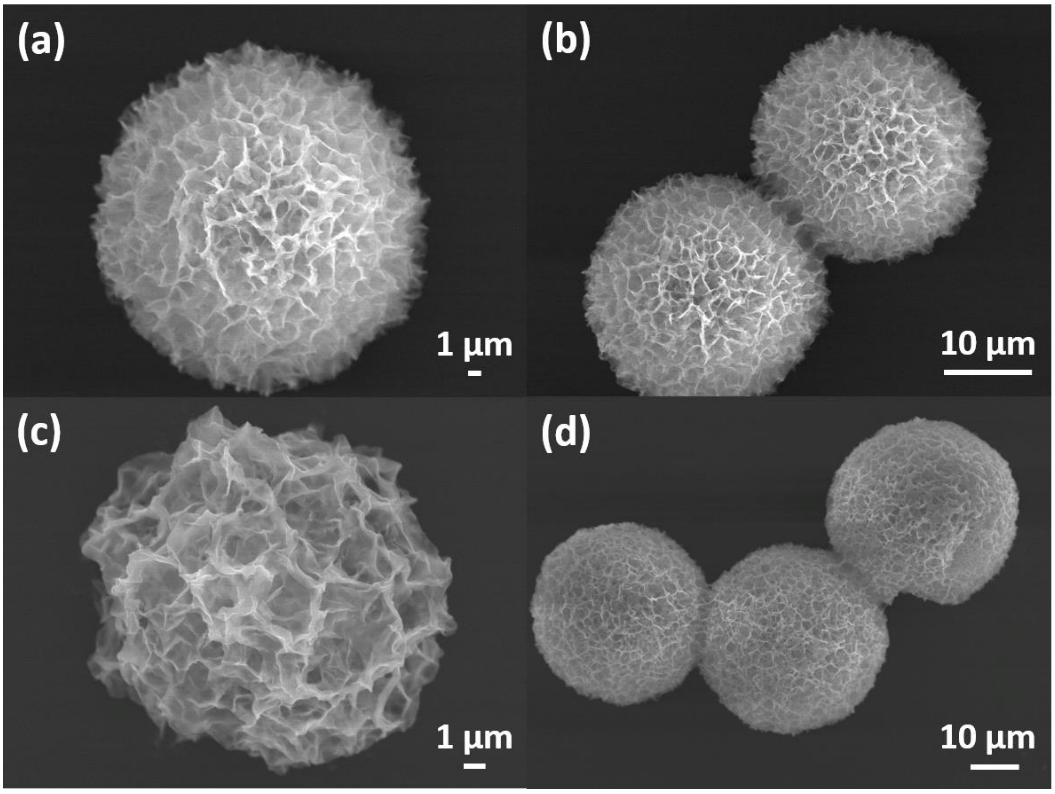

Fig. S24. FSEM images of **1-Xerogel** after 24h immersed at pH 4.5 (left) and pH 6.0 (right) buffer solutions at 25 °C.

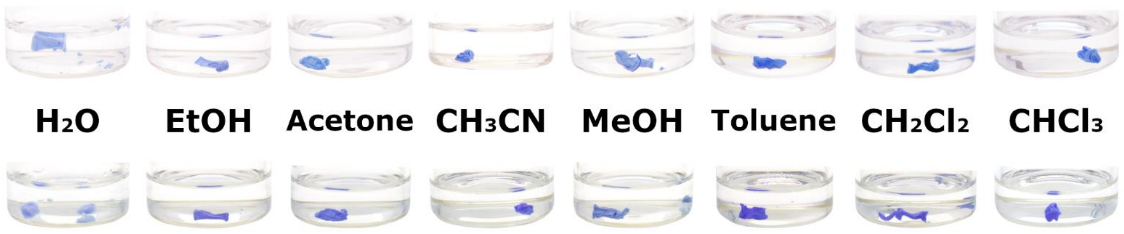

Fig. S25 1n-Xerogel immersed in different solvents recently prepared (up) and after one week (down).

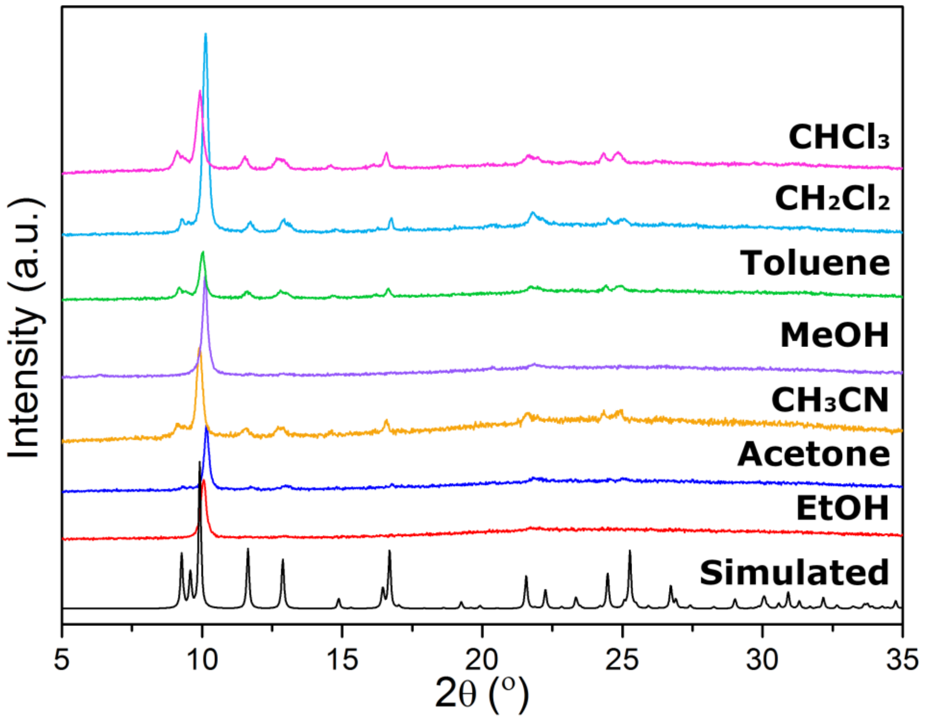

Fig. S26 X-ray powder diffraction patterns of simulated and **1n-Xerogel** after 1 week immersed in different solvents.

Physical Properties

Mechanical Compression Tests

An INSTRON 5967 testing device with a 20 N load cell was used to record compression-strain curves of cylindrical aerogel specimens. Physical features of the tested samples are gathered in Table S3. All specimens were compressed to a maximum force of 18 N at a rate of 5 mm min^{-1}, without exhibiting failure upon the explored range.

Stress-strain curves are gathered in Figure S28a, while Young modulus curve fitting and data are gathered in Figure S28b and Table S4.

Table S3. Physical features of **1n-Aerogel** specimens of compression tests.

Sample	Mass (g)	Shape	H (mm)	D (mm)	A (mm^2)	V (cm^3)	ρ (g·cm^3)
46	0.0760	cylinder	10.6	20.1	317.3	3.347	0.0227
49	0.1596	cylinder	12.6	24.5	471.4	4.849	0.0329
50	0.1593	cylinder	11.9	25.0	492.1	4.679	0.0340

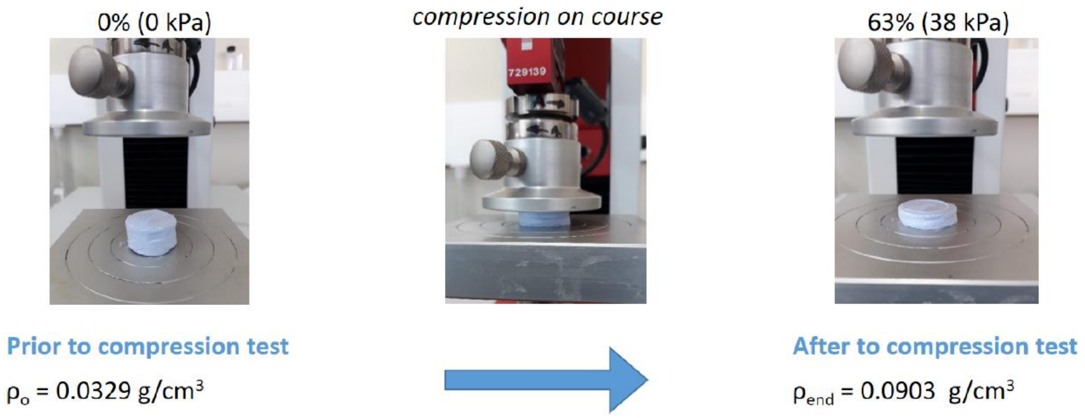

Fig. S27. Images acquired during the compression tests of **1n-Aerogel**.

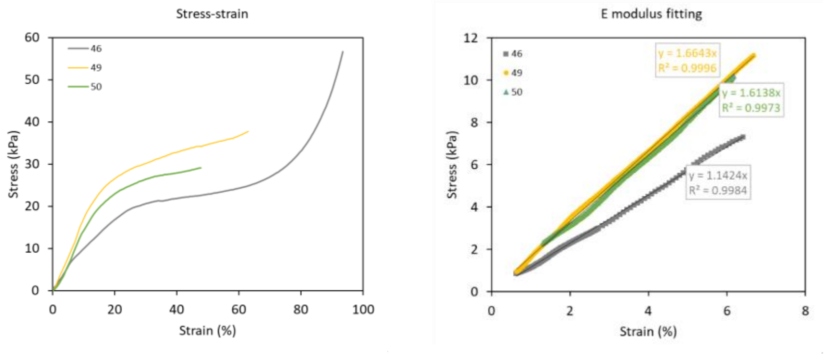

(a) (b)

Fig. S28 (a) Compression-strain curves performed on **1n-Aerogel** specimens. (b) Corresponding fittings for the estimation of the Young's modulus.

Table S4. Elastic modulus of **1n-Aerogel** specimens.

Sample	E (kPa)	$E_{specific}$ (kPa·m^3·Kg^{-1})
46	114.24	5.03
49	166.43	5.06
50	170.99	5.02

N_2 Adsorption Experiments

All physisorption measurements were performed on a Quantachrome Autosorb-iQ-MP. Prior to N_2 adsorption measurements all samples where outgassed under vacuum at 50 °C for 6 hours. Figure 6 of the main text shows the N_2 adsorption isotherms at 77 K, while the subtracted adsorption data is gathered in Table S6. All curves resemble a type II isotherm indicative of a dominating macroporosity. The sample exhibits certain contribution of microporosity which can be ascribed to the presence of narrow interlamellar cavities in the aerogel microstructure.

Table S6. Surface area, lamella thickness and pore volume data.

Sample	S_{BET} [a] (m^{2}g^{-1})	$D_{lamella}$ [b] (nm)	S_{micro} [c] (m^{2}g^{-1})	V_{micro} [c] (cm^{3}g^{-1})	V_T [d] (cm^{3}g^{-1})
1n-Aerogel	21.1	52.08	1.4	<0.001	0.088

[a]: BET specific surface area. [b]: lamella thickness; see calculation details below. [c]: micropore surface area (*S_{micro}*) and volume (*V_{micro}*) are estimated from the *t*-plot calculation. [d]: total specific pore volume (*V_T*) are computed at P/P_0 = 0.93 and 0.99 to account for pores smaller than 50 and 200 nm, respectively.

Calculation of lamella thickness

As the coordination polymer lacks intrinsic porosity, the specific surface area (ST) can be approached as the product of the number of particles per sample gram (Np) and the particle mean area (Sp) (Equation 1).[7] Since the number of particles can be calculated from the ratio between specific sample volume and particle mean volume (Vp) Equation 1 can be rewritten as Equation 2, where the specific volume has been replaced by the specific density (ρ).

$$S_T = S_p x N_p \qquad \textit{Equation 1}$$

$$S_T = \frac{S_p}{\rho \cdot V_p} \qquad \textit{Equation 2}$$

When particles are spherical or resemble regular polyhedrons, particle diameter or size can directly be derived. In principle it is not a useful equation for irregular polyhedrons as they are defined by more than one variable parameter, unless certain approaches are made. In this sense, the lamellar shape of the nanocrystal comprising the aerogels, imply that the lateral dimensions (L1 and L2) are much greater than the the thickness ($d_{lamella}$). Thus, the contribution of the lamella edges to the particle area can be discarded and lamella thickness can stimated from Equation 3.

$$d_{lamella} = \frac{2}{\rho \cdot S_T} \qquad \textit{Equation 3}$$

Note that herein we used the density value measured by He picnometry (1.82 g·cm^3).

Mercury Intrusion Experiments

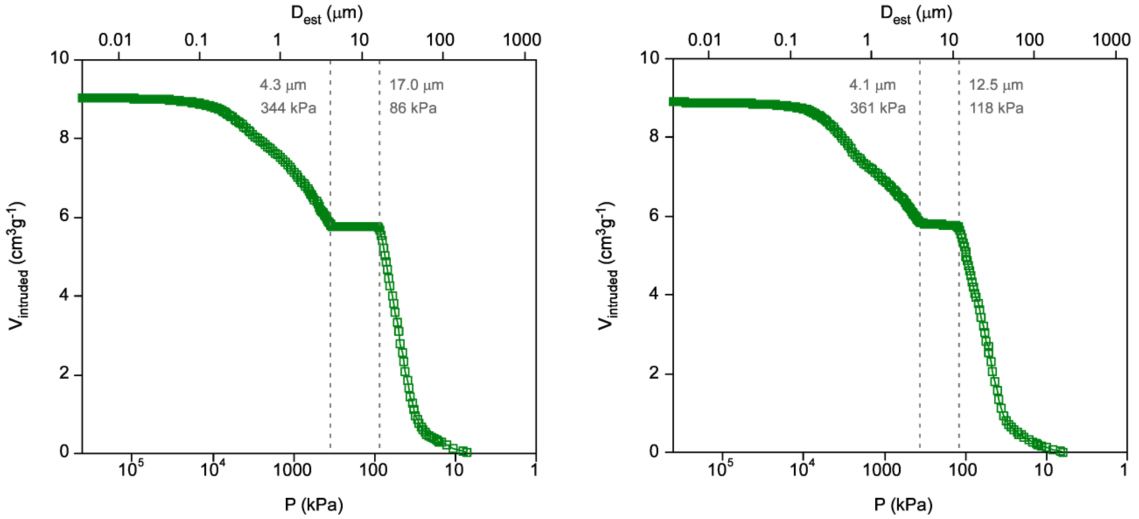

Sample 1

Sample 2

Fig. S29 Mercury porosimetry curves of **1n-Aerogel.**

References

1. M.-C. L. and J.-X. Y. J. Xiong, *Acta Cryst.* , 2005, **E61**, o2665.
2. G. C. A. Altomare, C. Giacovazzo and A. Guagliardi, *J. Appl. Cryst.* , 1993, **26**, 343.
3. G. M. Sheldrick, 1997, Program for Crystal Structure Refinement; University Gottingen, Gottingen (Germany).
4. G. M. Sheldrick, *Acta Cryst.*, 2015, **A71**, 3-8.
5. M. J. Prakash and M. S. Lah, *Chem. Commun.*, 2009, 3326.
6. G. A. Bain and J. F. Berry, *J. Chem. Edu.* 2008, **85**, 532.
7. G. Herdan, *Nature*, 1950, **165**, 858.